Conceptual design of supermirror polarizers at the European Spallation Source

Damián Martín Rodríguez[1*], *Peter* Willendrup[1, 2], *Wai-Tung* Lee[1], *Alex* Backs[1, 3], *Félix* Jiménez Villacorta[4], *Rasmus* Toft-Petersen[1, 2], and *Manuel* Morgano[1]

[1]European Spallation Source ERIC, Partikelgatan 2, 22484 Lund, Sweden
[2]Technical University of Denmark, Anker Engelunds Vej 101, 2800 Kongens Lyngby, Denmark
[3]Lund University, Division of Materials Engineering, Ole Römers väg 1, 22363 Lund, Sweden
[4]ESS-Bilbao, Parque Laida Bidea, Edificio 207-B, 48160 Derio, Spain

Abstract. Polarized neutrons will be made available on many European Spallation Source (ESS) instruments. There are a number of technologies available for polarizers and polarization analyzers which will be used at the ESS. The selection of the technology for an instrument is based on the performance and the constraints of the instrument. We will focus on the design of polarizing supermirror devices using Monte Carlo ray tracing simulation as an integral part of instrument design process. A McStas module has been developed to simulate a multichannel V-cavity polarizer, seeking the appropriate parameters to be incorporated into the respective instrument. The performance of such polarizers is studied for three instruments at ESS (MIRACLES (backscattering spectrometer), BIFROST (indirect geometry spectrometer) and ODIN (imaging)) with different requirements and constraints, where the suitability of this kind of devices can be assessed. For the first two instruments, where there is no strong constraint on the placement of the polarizer, the optimal configurations show excellent performance over the whole required wavelength ranges. However, in ODIN, due to more strict constraints in the placement of the polarizer, the performance is more dependent on the wavelength in the required wavelength range and other options may need to be considered.

1 Introduction

Polarized neutrons have been used in many applications for research using neutron scattering techniques [1] and have enabled a wider science case in many facilities. They also have enabled new experimental techniques like those using Larmor precession encoding [2].

There are different technologies available to polarize the neutron beam like polarizing supermirrors [3], polarized ^{3}He neutron spin filters [4] and Heussler monochromators [5] among others. The choice will depend on the requirements and constraints of the instrument (To be discussed in Section 2).

In the specific case of the European Spallation Source (ESS), an instrument suite has already been defined and it is being constructed [6]. In many instruments, the scope has to be reduced and incorporate the use of polarization for a later time. This imposes certain constraints in the choice of technology and needs careful design to still have a competitive performance.

In this work, we will present the design of the polarizer for three instruments: MIRACLES (backscattering spectrometer) [7], BIFROST (indirect geometry spectrometer) [8] and ODIN (imaging) [9].

MIRACLES is a backscattering spectrometer that is located with other long instruments at ESS, where the sample position is around 160 m away from the moderator. Therefore, it has a long guide [10] where a polarizer can be placed where the beam is less divergent, ensuring a high polarization at the required operating wavelength range. The inclusion of polarization analysis in backscattering instruments is becoming more important and would enhance the current capabilities of the instruments [11].

The case of BIFROST is very similar as the case of MIRACLES in terms of constraints. Located in the same area, and at a similar distance from the moderator, it also has certain flexibility in the placement of the polarizer, and also can be included where the beam is less divergent. The inclusion of a polarization analysis setup with a convenient analyzer technology, like the one proposed by P. Böni [12], would be beneficial for increasing the capabilities of the instrument.

In contrast to the other cases, the constraints in the ODIN beamline are stricter as it is a shorter instrument with a complex chopper cascade, which gives less flexibility to place the polarizer where the beam is less divergent. In addition to that, unlike the other two cases, the sample size is bigger and imposes an additional requirement of a polarized beam over a large region. The inclusion of polarized imaging will enhance the capabilities of the instrument further [13].

For the purpose of designing the polarizers, Monte Carlo ray-tracing codes [14, 15] are an essential tool,

* Corresponding author: damian.rodriguez@ess.eu

providing important insight to facilitate the best design choice to achieve the performance requirements.

2 Technical considerations, simulation method and design principles

Within the project to provide polarization at ESS [16] there are different technologies considered for polarization. There is going to be shared equipment for ^{3}He polarization, but some instruments can explore the possibilities for supermirror polarization. ^{3}He polarization has an important advantage that it can adapt to many beam characteristics (with more or less divergence) as the cell containing the ^{3}He gas can be manufactured in different geometries. On the other hand, supermirror polarizers need specific beam characteristics, like low beam divergence, in order to have a good polarization performance. However, supermirror polarizers have the advantage of being passive elements that can produce polarized neutrons after the polarizer is placed accurately in the beam. In the case of ^{3}He polarization, it needs some time to be set up before the experiment as the gas needs to be polarized by optical pumping and polarization can change as a function of time. In the case of MIRACLES and BIFROST, as it will be discussed below (figs. 4 and 8), the choice of supermirror polarizers is obvious as it can be placed where the neutron beam has low divergence. In the case of ODIN, with the limitation of placing the polarization in the cave, this is not that obvious and it is worth exploring this possibility to use the advantages of supermirrors while minimizing its inconveniences. The requirements coming from the instruments are summarized in Table 1.

Table 1. Requirements for the polarizers

* Field of view at 5 m from the pinhole position

Instrument	Operating Δλ (Å)	Minimum polarization	Sample size (cm^2)
MIRACLES	5.0 – 7.0	0.95	3.0 x 3.0
BIFROST	2.0 – 6.0	0.95	3.0 x 3.0
ODIN	2.5 – 7.5	0.95	10.0 x 10.0 *

All the three instruments have requirements of a neutron beam with a high degree of polarization for the wavelength range where they have to operate (see third column in table 1). To work with the pre-determined beam line geometry, a transmission geometry of the polarizer is chosen as it does not change the characteristics of the beam going through the polarizer. The use of V-cavity geometry [17] has the advantage of providing beam uniformity, and in its multichannel version [18] it makes it more compact.

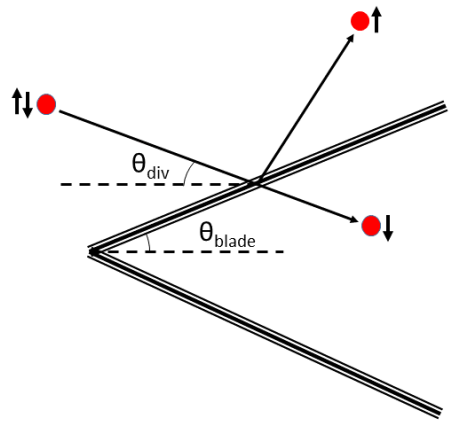

Fig. 1. Sketch of the neutron going through a supermirror polarizing cavity. For a polarizing supermirror, the incoming neutron beam is split into a reflected spin-up (polarized parallel to the applied saturated magnetic field) and a transmitted spin-down beam (polarized anti-parallel to the applied saturated magnetic field) spin state.

Fig. 1 shows the schematics on how the polarizing cavity works. The neutrons with the correct spin state will go through the mirror with the divergence distribution unchanged while the ones with the wrong spin state will be reflected with a higher divergence. In the case of the reflected beam we have two cases. In the case where the polarizer is placed within the guide system, the reflected beam's angle is higher and will be absorbed by the guide system, especially in its focusing section, until certain wavelength, where the critical angle is high enough to allow more divergent beams to be transported. Of course, multiple reflections within the polarizer also means that the surviving beam will be even more divergent, and therefore, its transport through the guide system will take place at even higher wavelengths. Furthermore, as the reflectivity for spin down (i. e., the wrong spin state) has $m < 1$, there will be a cut-off wavelength where total reflection of the beam in the cavity will take place [19]. We have checked that in the case of MIRACLES and BIFROST (which have long focusing sections of more than 10 m long) for the wavelengths they have to operate (table 1, third column) only the beam with the correct spin state reaches the sample position. In the case of ODIN, where the polarizer will be placed in the cave (see below, fig. 12), both contributions will be separated when arriving to the sample, and therefore, there is enough space to shield the beam with wrong spin state.

McStas code has been extensively used for the design of many instruments in different facilities around the world and it has been the preferred choice of software for the teams building the studied instruments. The simulation files of the instrument guide systems have been provided by the instrument teams and is the basis to add the polarizers in the instrument files.

In these simulations we used the McStas 2.7.1 version and two components had to be modified in order to perform this study. First, the polarizing cavity component available for McStas (*Pol_guide_vmirror*) was modified in order to allow multiple cavity channels. A new parameter has been added to specify the number of channels of the polarizer. This modification has been

included in the following version (McStas 2.7.2). The second modification was the development of the component to obtain polarization maps (*PSD_pol_monitor*), which was not available in the McStas and has been developed by one of the co-authors (Alex Backs). This component has not been included yet, but there are plans to do it in the near future.

First of all, the V-cavities are constructed with Si blades which are coated from both sides. This is done to improve the polarization and to compensate the internal stresses of the wafers. Therefore, as an initial approximation we will use the reflectivity curve of a double mirror in the simulation, i. e., the reflectivity of the neutron going through two single reflective surfaces with the same layer sequence. This may not be accurate, but as a first approximation it will fulfil the aim of the study to find trends of different parameters and choose the optimal ones for the polarizers.

It is important to consider that the *Pol_guide_vmirror* component has an important limitation. Polarizing mirrors and cavities are sputtered over a Si wafer with a thickness of around 300 µm. The Si wafer will have some absorption that can be quantified but it is not taken into account in the component. It is possible to calculate the contribution of the absorption using different resources [20-22] and Fig. 2 shows the dependence of the penetration depth of the Si (the thickness needed to attenuate the incoming intensity by a factor 1/e) as a function of the neutron wavelength.

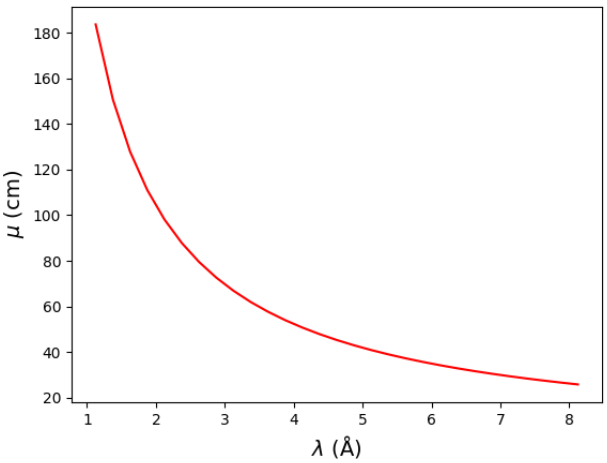

Fig. 2. Penetration depth (µ) of the Si as a function of the incoming neutron wavelength.

In this way, we can roughly estimate the absorption of the Si wafer.

The transmission T will be calculated as the ratio between the intensity of the beam at the sample position and area (defined in table 1, fourth column) with the polarizer and without the polarizer. Assuming that the incoming neutron beam has no divergence, the corrected transmission can be calculated as:

$$T_{corr} = T \exp(-t / (\mu \sin \theta_{blade})) \quad (1)$$

where t is the substrate thickness and θ_{blade} is the angle of the polarizing cavity blade. The assumption made to derive the equation is more accurate in the case of a low divergence beam at the polarizer as the differences in thickness are low. This is not happening for higher divergences, but it will give an initial approximation on the effect of absorption.

A feature not taken into account in the simulation are the separators between channels in the V-cavities, as it appears, for example, in Ref. 18. If the separators are absorbing, there is going to be an additional decrease on transmission that is not taken into account in the simulations. These will depend on the number of channels and length of the polarizer.

Another important factor that is not taken into account in the simulations are the depolarization effects in supermirrors [23]. These come from the off-specular scattering in the multilayers and can be reduced by applying a magnetic field. The required strength of the magnetic field will depend on different factors like the angle and the m index of the coating. According to the results in Ref. 22, a magnetic field of around 30 mT is enough to reduce these depolarization effects to an acceptable level, but it will increase for high m coatings.

In addition to that, guide fields have to be designed to reduce depolarization effects during the path from the polarizer to the sample, which requires careful design using finite elements calculations. These are out of the scope of this work and the simulation considers that there is no depolarization in the path to the sample.

The choice of the type of polarizing mirror used in the device can be important. Fe/Si supermirrors [3] are widely used as a good compromise between performance and cost. In addition to that, they have no activation issues like the mirrors containing Co.

The inclination of the blades (θ_{blade}) will be calculated using a criterion of high polarization over the operating wavelength range. The formula to estimate the needed inclination of the blades in degrees is as follows:

$$|\theta_{blade}| = m \times \lambda_c \times 0.1° - |\theta_{div,max}| \quad (2)$$

Where m is the critical angle of the coating expressed as a function of the critical angle of Ni, λ_c is the critical wavelength where the reflectivity will be high (which will be slightly lower than the lowest limit of the operating wavelength range of the instrument) and $\theta_{div,max}$ is the maximum divergence of the beam.

The design considerations are simpler than in the study made by Dewhurst [24], where the maximum divergence of the beam has a linear dependence with wavelength. This study takes the assumption of extended source geometry and straight guide geometry, which is not the case at ESS. The moderator at ESS uses a complex geometry with thermal and cold zones with a reduced dimensionality in the vertical direction in order to increase the brightness of the source [25]. As in the design of MIRACLES and BIFROST guides [8, 10], the low dimensionality of the moderator in the vertical direction enables extracting the beam with a defocusing elliptical guide section, converting it into a lower divergence beam with no wavelength dependence. In the case of the of the horizontal divergence, a defocusing guide can be placed after the curved section used to filter fast and epithermal neutrons. Therefore, it is possible to obtain a value of the maximum divergence which is independent of the wavelength, making the optimization easier.

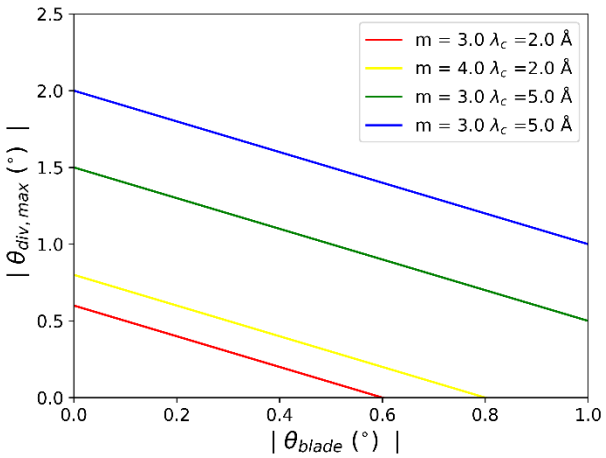

Fig. 3. Evolution of θ_{blade} as a function of $\theta_{div,max}$ as described in equation (2) for different examples.

The trends of equation (2) are shown in fig. 3. For given values of m and λ_c, the values of θ_{blade} depend linearly with $\theta_{div,max}$. In terms of manufacturing, a low value of θ_{blade} would imply a larger surface to coat and more channels, which would increase costs and would be more difficult to manufacture. However, increasing the m coating also can increase the costs. Therefore, a compromise has to be reached.

3 Results and discussion

3.1 Polarizer for instrument MIRACLES

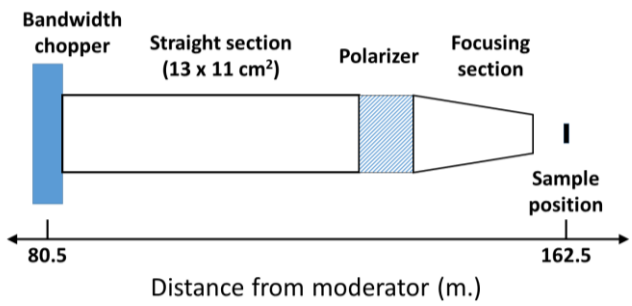

Fig. 4. Sketch of the location of the polarizer of MIRACLES instrument

Fig. 4 shows the location of the polarizer within the guide system of MIRACLES. After the bandwidth chopper there is long straight section with a large cross section (13 × 11 cm^2) before it starts the focusing section. The straight section also has a coating of m = 1.5 in all the sides. The focusing section will be an elliptic guide section that will focus the beam to the sample. The beam with wrong spin state will be absorbed by the focusing part within the operating wavelength range.

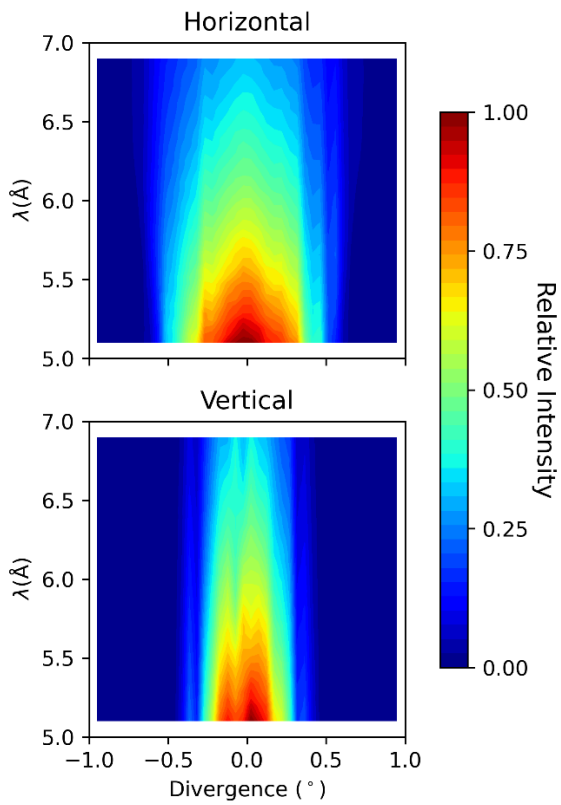

Fig. 5. Divergence distribution as a function of the wavelength of the neutron beam at MIRACLES before the polarizer.

Fig. 5 shows the divergence distribution as a function of wavelength in both horizontal and vertical direction before the polarizer. It shows that in the case of the vertical direction the maximum divergence is smaller and is wavelength independent. In the case of the distribution in the horizontal direction, the maximum divergence is larger and has a slight dependence with wavelength. If we take into account the trends in fig. 3, where it is important to seek a large θ_{blade}, a small maximum divergence would be more beneficial, apart from a wavelength independent divergence distribution. For this reason, the mirrors of the cavity will be vertically arranged (i. e., where the plane of the mirrors contains the horizontal direction axis) and therefore, in the calculation of equation (2) we will take $\theta_{div,max} = 0.3°$. In addition to that, we will use λ_c = 4.5 Å, in order to obtain the required polarization at the operating wavelength range.

Table 2. Parameters of the simulated polarizers for MIRACLES

m	θ_{blade}(°)
2.4	0.78
2.6	0.87
2.8	0.96
3.0	1.05

Table 2 shows the parameters of the simulated polarizers. In order to observe the angular dependence of the performance, we will also perform simulations for each polarizer with values of $\theta_{blade} \pm 0.02°$ for a given value of m. This will be represented in the following figures as a shade. The polarizers will be simulated as single channel as the optimal length will be later determined by the engineering requirements and constraints. The total length of the device will depend on the available space and a compromise has to be reached in order to have feasible alignment requirements. Of course, beam losses due to channel separators have to be considered in further studies. The polarizer will have the V-cavity pointing upstream.

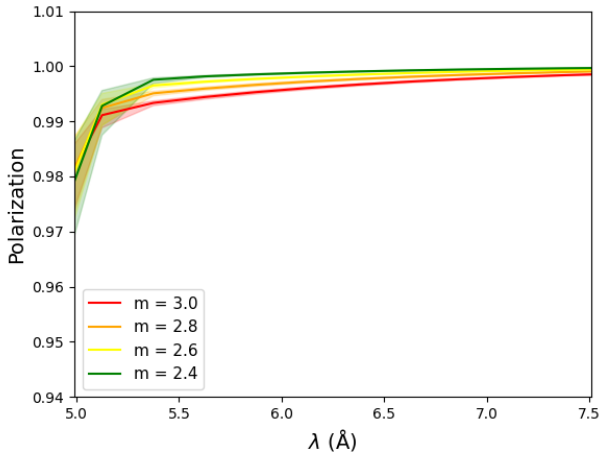

Fig. 6. Polarization at the sample position as a function of wavelength for the simulated polarizers in MIRACLES described in table 2. The shady areas show the variation of the polarization modifying the nominal θ_{blade} shown in table 2 in a range of ± 0.02°.

Fig. 6 shows the polarization of the simulated polarizers described in table 2 as a function of wavelength. The shady areas show variations in the polarization performance if θ_{blade} is modified in the range of ± 0.02° from the nominal value. In this case, all the studied polarizers produce a neutron beam with the required polarization. The curves look very similar and variations in θ_{blade} still fulfil the requirements.

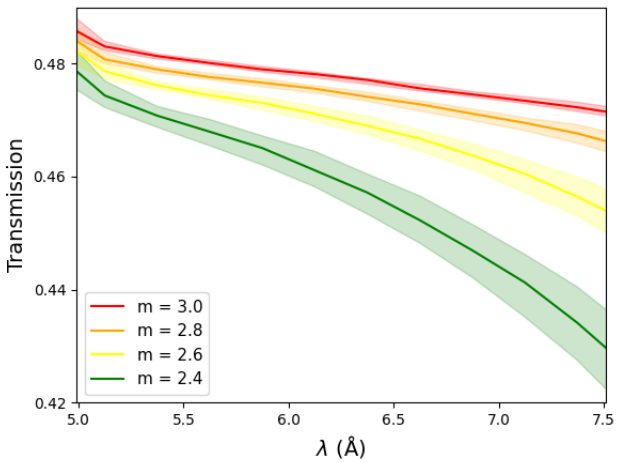

Fig. 7. Corrected transmission at the sample position as a function of wavelength for the simulated polarizers in MIRACLES described in table 2. The shady areas show the variation of the transmission modifying the nominal θ_{blade} shown in table 2 in a range of ± 0.02°.

Fig. 7 shows the corrected transmission (i. e., the transmission taking into account the Si absorption) as a function of the wavelength for the studied polarizers. As in fig. 7, the shady areas correspond to the variations in transmission performance if θ_{blade} is modified in the range of ± 0.02° from the nominal value found in table 2. For this case, the transmission curves have a strong variation. While the polarizer with m = 3 has a high transmission for the whole operating wavelength range, in the case of m = 2.4, it decreases continuously. The angular variation in transmission also changes as a function of m. The polarizer with m = 2.4 has a strong variation with θ_{blade}, but that is not the case with the polarizer with m = 3.

The results in MIRACLES show that in all cases, a high degree of polarization is achieved. However, the main driving difference in the performances of the polarizers is in its transmission. In order to achieve a competitive performance for the instrument the polarizer with m =3 would be the best option among the ones analyzed as it would also have a competitive transmission beyond the operating wavelength range (between 5 – 7 Å) in order to analyze the tail of the quasielastic peak (from 7-8 Å). In addition to that, the variation with angle is the lowest, as it has a negligible shade (see fig. 7), making it also more robust against the effects of surface waviness of the blades. A higher m would extend the range with high transmission, but it would not widen the science case of the instrument.

3.2 Polarizer for instrument BIFROST

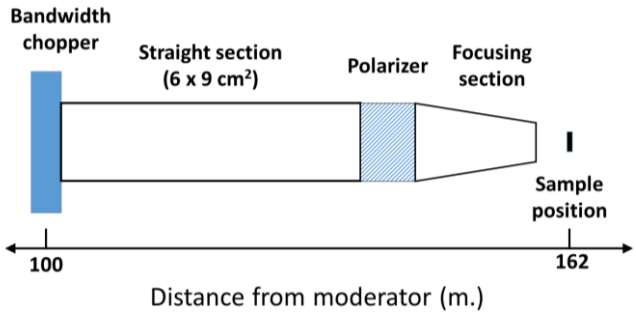

Fig. 8. Sketch of the location of the polarizer of BIFROST instrument

As it is shown in fig. 8, the case of BIFROST is also very similar to MIRACLES, where there is a long guide section after the last bandwidth chopper. In this case, the straight guide has a cross section of 6 x 9 cm^2. After that, a focusing section follows before the neutron beam reaches the sample position. The guide section enclosing the polarizer has a coating of m = 2.

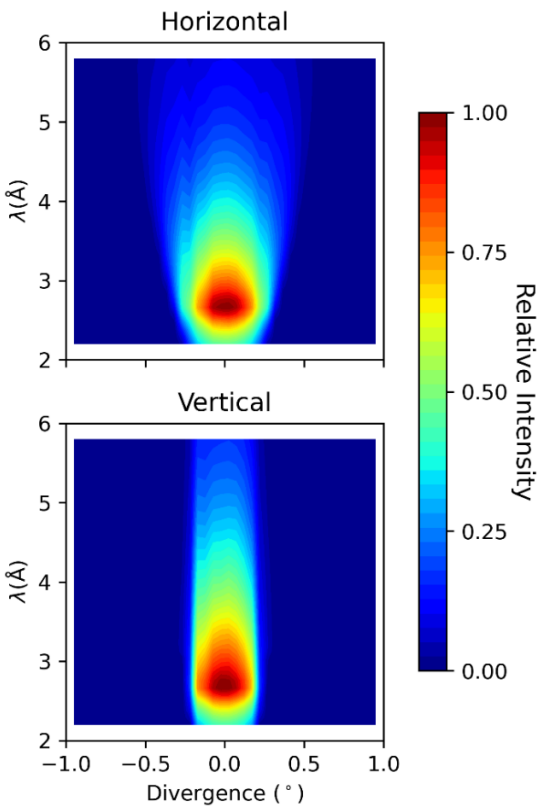

Fig. 9. Divergence distribution as a function of wavelength of the neutron beam at BIFROST before the polarizer.

Fig. 9 shows the divergence distribution as a function of wavelength in both horizontal and vertical direction before the polarizer. It can be argued in the same way as in MIRACLES that it is more convenient to have the mirrors of the cavity vertically arranged and therefore $\theta_{div,max} = 0.2°$. In addition to that, we will use $\lambda_c = 2.0$ Å, in order to obtain the required polarization at the operating wavelength range.

Table 3. Parameters of the simulated polarizers for BIFROST

m	θ_{blade}(°)
3.5	0.50
3.8	0.55
4.0	0.61
4.2	0.64
4.4	0.67
4.6	0.72

Table 3 shows the parameters of the simulated polarizers where the angle of the blades is proportional to the *m* of the coating. In an analogous way, we will also simulate the systems with $\theta_{blade} \pm 0.02°$ for a given value of m in order to observe the dependence with the angle of the blades.

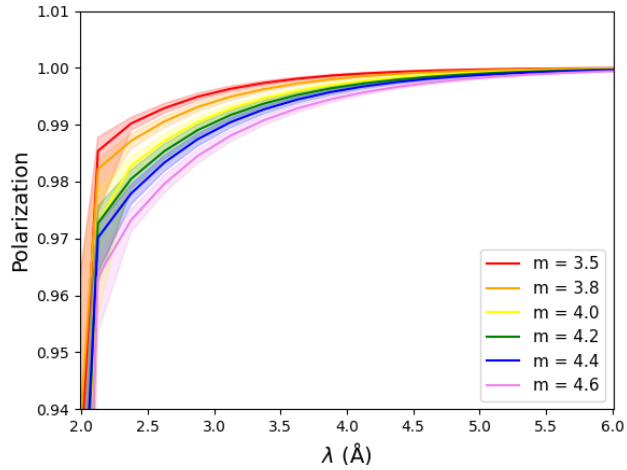

Fig. 10. Polarization at the sample position as a function of wavelength for the simulated polarizers in BIFROST described in table 3. The shady areas show the variation of the polarization modifying the nominal θ_{blade} shown in table 3 in a range of ± 0.02°.

Fig. 10 shows the polarization as a function of the wavelength for the polarizers described in table 3. Polarization is within requirements in all the simulated polarizers. Even varying θ_{blade} in the range of ± 0.02° the polarizers also fulfil the performance requirements.

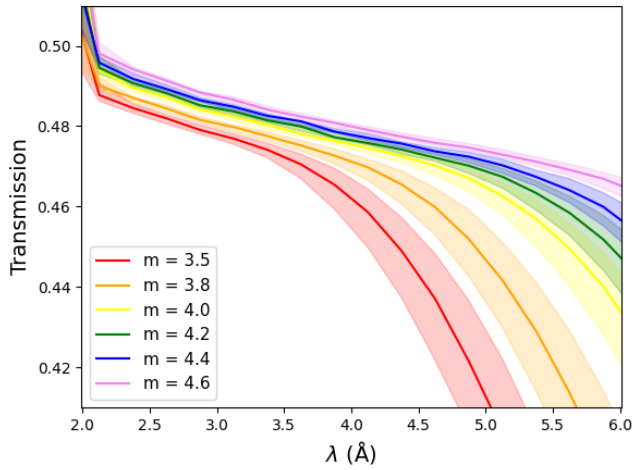

Fig. 11. Corrected transmission at the sample position as a function of wavelength for the simulated polarizers in BIFROST described in table 3. The shady areas show the variation of the transmission modifying the nominal θ_{blade} shown in table 3 in a range of ± 0.02°.

Fig. 11 shows the transmission as a function of the wavelength for the studied polarizers for BIFROST. It follows the same trend as in fig. 7 where the polarizers with higher *m* coating have a high transmission over a longer wavelength range

In the case of BIFROST, despite the strong equivalence with MIRACLES, it is also important to take into account other factors like the cost, as the *m* of the coatings is higher than in the former case of MIRACLES. All the studied polarizers obtain the required polarization, but the transmission is different. The polarizer with the highest transmission over the whole operating wavelength range (between 2 – 6 Å) is the one with the highest *m*, but the ones with $m \geq 4.0$ have little differences in transmission of a maximum 4 %, and therefore a good compromise between cost and

performance could be the one with m = 4.2. However, this choice should be reviewed when official quotations with the manufacturers are taken into account, together with the available budget.

3.3 Polarizer for instrument ODIN

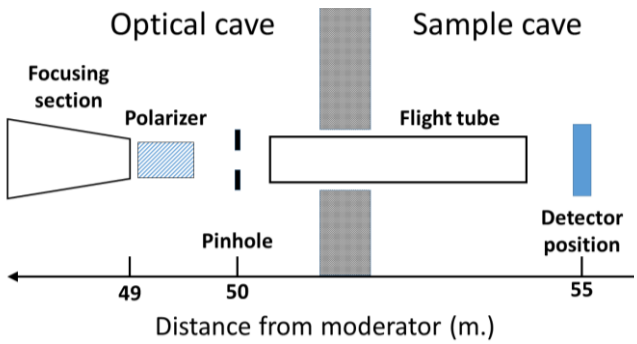

Fig. 12. Sketch of the location of the polarizer of in the ODIN instrument cave.

The case of ODIN is completely different and the polarizer has to be placed in the cave. Fig. 12 shows a sketch of the cave where the polarizer is placed. The cave is divided in two parts. The Optical cave has the end of the guide system and the pinhole that adjusts the beam shape before going to the sample (in this case the 3 x 3 cm^2 pinhole has been chosen). The flight tube after the pinhole creates vacuum to minimize neutron losses This communicates with the Sample cave, where the sample and the detector will be placed at varying distances. The most convenient location to place the polarizer is at the end of the guide and the length will be limited at 50 cm at most in order to avoid clashes with the pinhole. The enclosing around the polarizer mirrors is absorbing.

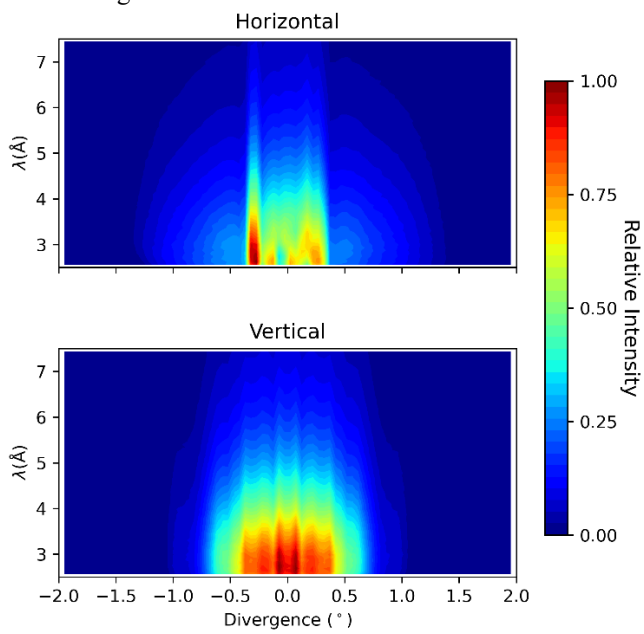

Fig. 13. Divergence distribution as a function of wavelength of the neutron beam at ODIN before the polarizer.

As in the other cases, fig. 13 shows the divergence distribution as a function of the wavelength. As the beam is after a focusing section of the guide, the beam has a larger divergence than in the former cases.

With the current multichannel v-cavity geometry, observing the trends of fig. 3, there wouldn't be any value of θ_{blade} available for such a high divergence and equation (2) would be negative, which makes no physical nor mathematical sense. An alternative solution would be to simply polarize part of the beam, and therefore use different lower values of $\theta_{div,max}$ for the calculation of θ_{blade}.

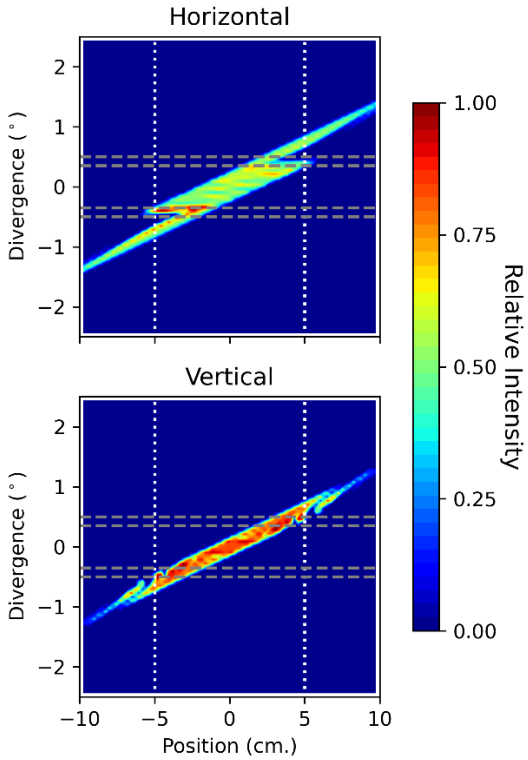

Fig. 14. Acceptance diagrams in both dimensions of the neutron beam at the detector position without polarizer. The greydashed lines denote the different values of $\theta_{div,max}$ taken for the design of the simulated polarizers (see table 4) and the white dotted lines show the spatial limits of the detector.

In fig. 14 we can can observe the acceptance diagrams in both directions of the unpolarized beam (that is, without placing any polarizer) integrated over the operating wavelength range where the white dotted lines are the spatial limits of the detector and the grey dashed lines are the values of $\theta_{div,max}$ chosen for the designs.

As can be seen, if only part of the beam is polarized, the higher divergence part of the beam that is not polarized by the polarizer would still degrade the polarization at the sides of the detector. However, taking into account that the critical angle of the coatings is wavelength dependent, we can ensure high levels of polarization by choosing a value of λ_c in eq. (2) lower than the lower limit of the operating wavelength range (2.5 Å). This way, we could ensure that the whole phase space within the detector area reaches a high level of polarization. In our case we have chosen λ_c = 2.0 Å. This strategy works better in the vertical direction, where the phase space has an approximate shape of a rhomboid. In the horizontal direction we can observe some contributions in higher divergence where this strategy would be more difficult to apply and the results would show a higher degree of degradation in the sides.

Therefore, the blades of the polarizer will be arranged vertically.

Table 4. Parameters of the simulated polarizers for ODIN

m	$\theta_{div,max}$ (°)	θ_{blade} (°)	Length (m)	channels
4.0	0.35	0.45	0.47	4
4.0	0.50	0.30	0.47	6
4.5	0.35	0.55	0.39	4
4.5	0.50	0.40	0.43	5

Table 4 shows the parameters of the simulated polarizers for ODIN. In this case we use a compact multichannel arrangement for the simulations.

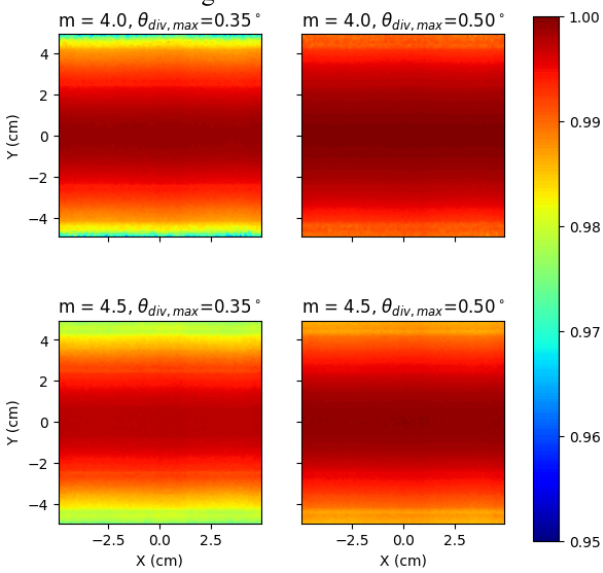

Fig. 15. Spatial distribution of polarization at the detector position of the different simulated polarizers for ODIN described in table 4.

The spatial distribution of the polarization in the detector is also important to analyse in order to ensure that the whole detector area has the required polarization. Fig. 15 shows the spatial distribution of the polarization integrated over the operational wavelength range for ODIN (2.5-7.5 Å). In all cases the total polarization is over 95 %, as required. In all cases, the highest polarization is in the center of the beam and it decreases when it goes towards the borders.

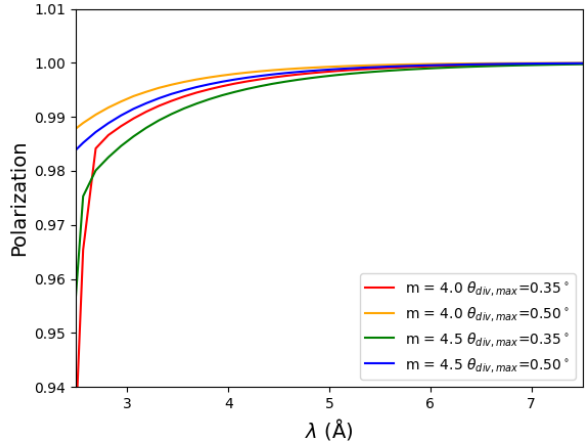

Fig. 16. Polarization at the sample position as a function of wavelength for the simulated polarizers in ODIN described in table 4

Fig. 16 shows, as in the former cases, the polarization averaged over the whole detector area as a function of the wavelength. In all cases, the polarization is within the required value.

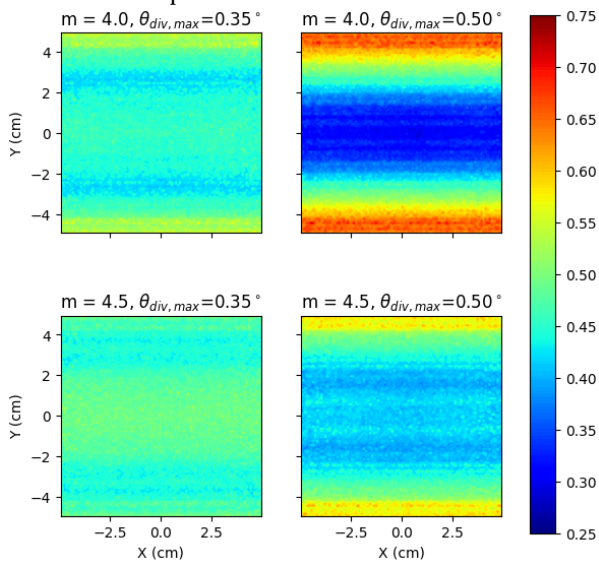

Fig. 17. Spatial distribution of the uncorrected transmission (see the text to see how it is calculated) at the detector position of the different simulated polarizers for ODIN described in table 4.

The spatial uniformity of the beam in the detector area is also important to study as, in general, beam uniformity is an important condition for imaging beamlines. It is important to analyze if the polarizer introduces additional inhomogeneities to the beam. For that purpose, we can use the ratio between the with the chosen polarizer and the beam without the polarizer. Fig 17 shows the spatial distribution of transmission in the simulated cases integrated over the operating wavelength range without applying the effect of Si absorption. There is are larger inhomogeneities created when increasing $\theta_{div,max}$ and decreasing m (and therefore, decreasing θ_{blade}). It also appears transmissions over 0.50 in some cases, which should be analyzed in further studies.

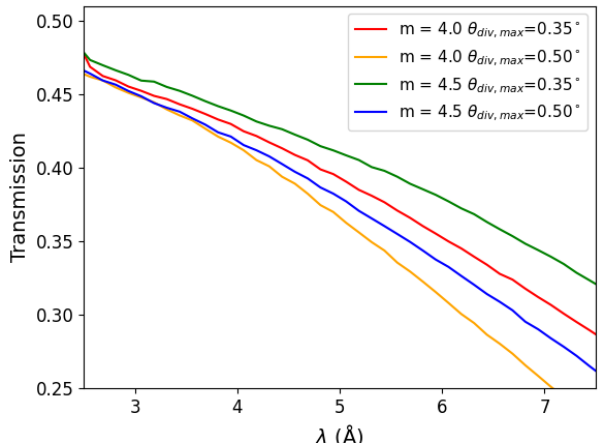

Fig. 18. Corrected transmission at the sample position as a function of wavelength for the simulated polarizers in ODIN described in table 4.

Fig. 18 shows the transmission at the detector position for the simulated devices. In all the simulated polarizers, the transmission is high for shorter wavelengths and the transmission decreases as a function of wavelength. In some cases, the transmission at the longer wavelength range can be lower than 0.30. It is also important to point out that transmission is better with increasing m but decreasing $\theta_{div,max}$.

Unlike the former cases, the results obtained for ODIN do not lead to an obvious technical choice to be implemented. Although the required polarization is obtained with a sufficient degree of spatial uniformity (figs. 15-16), the transmission is strongly dependent of the wavelength (fig. 18).

In addition to that, homogeneity of the beam is also important, and fig. 17 shows strong inhomogeneities in some of the cases that are not acceptable to conduct an experiment. It is also important to point out that, as the incoming beam is more divergent and the Si absorption is very dependent on the path through it, there may be additional inhomogeneities that are not taken into account in the simulation.

Despite not being able to find a conclusive solution for ODIN, the results indicate very important trends to find a more convenient solution. A higher *m* in the coating and a higher θ_{blade} in the polarizer produces a higher transmission and a higher uniformity in the beam arriving to the detector.

Taking into account these trends, a higher *m* than the ones analyzed in the study would improve the performance, leading to important increases in cost. In that case, other solutions would need to be explored in further studies, like for example a fan arrangement where each channel has a different angle or a logarithmic spiral geometry of the mirrors [26].

4 Conclusions

This study presents the conceptual design of the supermirror polarizers for three instruments at ESS: MIRACLES (backscattering spectroscopy), BIFROST (indirect geometry spectroscopy) and ODIN (imaging). All the three instruments have different requirements and constraints that have to be taken into account (see table 1). In all cases, it is studied the performance of polarizers in transmission geometry, as they perform better in the required operating wavelength range (table 1, column 3).

The cases of MIRACLES and BIFROST are very similar, as can be observed in figs. 4 and 8. The proposed solution places the polarizer in the guide system before the focusing section that both have. The optimal parameters have been found that ensures a high polarization and a high transmission (i. e., a higher flux at the sample position).

In the case of ODIN (fig. 12), the main constraint is that the polarizer has to be placed in the cave, where the beam is more divergent. Even if the polarization obtained at the detector position is within the requirements, transmission is lower than the other cases and strongly dependent on the wavelength. In addition to that, beam inhomogeneities have to be taken into account to find the most convenient solution. The trends in the results show that a higher *m* in the coating and a higher angle of the blades (θ_{blade}) lead to a higher transmission and a more uniform beam. This would lead to a solution with high costs pushing the technological limits of polarizing supermirror coating. Therefore, other solutions with different mirror arrangements will be explored in further studies.

References

1. W. G. Gavin, *Polarized Neutrons* (Clarendon Press, Oxford, 1988)
2. F. Mezei, C. Pappas, Th. Gutberlet eds., *Neutron spin echo spectroscopy* (Springer Berlin, Heidelberg, 2003)
3. J. Stahn, D. Clemens, Appl. Phys. A **74**, S1532 (2002)
4. K. H. Andersen, D. Jullien, A. K. Petoukhov, P. Mouveau, F. Bordenave, F. Thomas, E. Babcock, Physica B **404**, 2652 (2009), G. L. Jones, T. R. Gentile, A. K. Thompson, Z. Chowdhuri, M. S. Dewey, W. M. Snow, F. E. Wietfeldt, Nucl. Instrum. Methods Phys. Res. A **440**, 772 (2000).
5. P. Courtois, Physica B **267-268**, 363 (1999)
6. K. H. Andersen, D. N. Argyriou *et al.,* Nucl. Instrum. Methods Phys. Res. A, **957**, 163402 (2020)
7. N. Tsapatsaris, R. E. Lechner, M. Markó, H. N. Bordallo, Rev. Sci. Instrum. **87**, 085118 (2016)
8. M. Klausz, K. Kanaki, T. Kittelmann, R. Toft-Petersen, J. O. Birk, M. A. Olsen, P. Zagyvai, R. J. Hall-Willton, J. Appl. Cryst., **54**, 263 (2021)
9. M. Strobl, Phys. Procedia, **69**, 18 (2015)
10. F. J. Villacorta, D. Martin Rodriguez, M. Bertelsen, H. N. Bordallo, Quantum Beam Sci., **6**, 3 (2022)
11. K. Nemkovski, R. Bewley, V. Garcia Sakai, G. J. Nilsen, A. Perrinchon, I. Silverwood, EPJ Web Conf. **272**, 02004 (2022)

12. P. Böni, C. Schanzer, M. Schneider, Nucl. Instrum. Methods. Phys. Res. A **966**, 163858 (2020)
13. M. Dawson, I. Manke, N. Kardjilov, A. Hilger, M. Strobl, J. Barnhart, New J. Phys. **11**, 043013 (2009)
14. P. Willendrup, and K. Lefmann, J. Neutron Res. 22, 1-16 (2020).
15. P. Willendrup, and K. Lefmann, J. Neutron Res. 23, 7-27 (2021).
16. W.- T. Lee, J. Hagman *et al.. This issue.*
17. T. Krist, C. Lartigue, F. Mezei, Physica B **180-181** 1005 (1992)
18. R. R. Gainov, F. Mezei, J. Fuzi and M. Russina, Nucl. Instrum. Methods. Phys. Res. A **930**, 42-48 (2019).
19. T Bigault, G Delphin, A Vittoz, V Gaignon and P Courtois., J. Phys. Conf. Ser. **528**, 012017 (2014)
20. https://www.ncnr.nist.gov/resources/activation/
21. H. Rauch and W. Waschkowski (2003). Neutron Scattering Lengths in *ILL Neutron Data Booklet* (second edition), A.-J. Dianoux, G. Lander, Eds. Old City Publishing, Philidelphia, PA. pp 1.1-1 to 1.1-17.
22. V. F. Sears (2006). *Scattering lengths for neutrons* In Prince, E. Ed. *International Tables for Crystallography Volume C: Mathematical, Physical and Chemical Tables* Kluwer Academic Publishers, pp 444-454.
23. C. Klauser, T. Bigault, P. Böni, P. Courtois, A. Devishvili, N. Rebrova, M. Schneider and T. Soldner, Nucl. Instr. Meth. A **840**, 181-185 (2016)
24. C. D. Dewhurst, Nucl. Instr. Meth. A **683**, 16-23 (2012)
25. K. H. Andersen, M. Bertelsen, L. Zanini, E. B. Klinkby, T. Schönfeldt, P. M. Bentley and J. Saroun, J. Appl. Cryst. **51**, 264–281 (2018).
26. J. Stahn and A. Glavic, J. Phys.: Conf. Ser. **862**, 012007 (2017)